Evaluation of Dual-Frequency GBAS Performance using Data from Public Receiver Networks

Kazushi Suzuki, *NEC Corporation*
Sam Pullen, *Stanford University*
Per Enge, *Stanford University*
Takeshi Ono, *NEC Corporation*

BIOGRAPHIES

Kazushi Suzuki is an Assistant Manager in the Air Traffic Management and Navigation Systems Department of NEC Corporation in Fuchu, Tokyo, Japan. He received his B.S. and M.S. degrees in Electrical Engineering from Doshisha University in 1998 and 2001, respectively. He joined NEC Corporation in 2001. Since then, he has been working on GNSS-related projects including QZSS, MSAS, and GBAS. He is currently a Visiting Scholar at Stanford University.

Sam Pullen is a Senior Research Engineer at Stanford University, where he is the director of the Local Area Augmentation System (LAAS) research effort. He has supported the FAA and others in developing GNSS system concepts, requirements, integrity algorithms, and performance models since obtaining his Ph.D. from Stanford in Aeronautics and Astronautics in 1996. Based on this work, he was awarded the ION Early Achievement Award in 1999. In addition to GNSS, his research involves the general topic of system design and performance verification under uncertainty.

Per Enge is a Professor of Aeronautics and Astronautics at Stanford University, where he is the Kleiner-Perkins, Mayfield, Sequoia Capital Professor in the School of Engineering. He directs the Stanford University GPS Laboratory, where he has been since 1995. Per has received the Kepler, Thurlow and Burka Awards from the Institute of Navigation (ION) for his work. He is also a Member of the National Academy of Engineering as well as a Fellow of both the ION and the Institute of Electrical and Electronics Engineers (IEEE). He received his PhD from the University of Illinois in 1983.

Takeshi Ono is a Senior Manager in the Air Traffic Management and Navigation Systems Department of NEC Corporation. He received his B.S. degree in Astronomy from the University of Tokyo. He has been working in orbital dynamics and GNSS technology since 1981 on several generations of Japanese satellites, as well as MSAS, QZSS, and GBAS systems.

ABSTRACT

This paper examines the effectiveness of two proposed methods for dual-frequency smoothing in Ground Based Augmentation Systems (GBAS) based on data collected in 2010 by clusters of nearby receivers whose measurements are publically available. After an extensive search turned up no ionospheric anomalies, data from several clusters of CORS and IGS stations under nominal conditions was examined, and results from three of these clusters are presented. Across these clusters, the variation with regard to receiver noise and multipath errors is very large. However, in all cases, dual-frequency smoothing performed well and generally agreed with theoretical predictions. These results confirm that future multiple-frequency GBAS systems using these methods are practical as long as receiver multipath is controlled to the level of the best CORS and IGS receivers.

1.0 INTRODUCTION

Mitigating ionospheric anomalies has been the largest challenge to GBAS system development and certification. Extreme spatial gradients of ionospheric delays that occur rarely during such anomalies can cause large differential errors and could lead to loss of integrity if not detected or mitigated in some manner. This is difficult in today's single-frequency (L1-only) GBAS because detection of severe ionospheric gradients cannot be guaranteed before users are threatened. In the existing GBAS systems that support CAT I precision approach, the ionospheric threat is mitigated by inflating the broadcast integrity parameters (i.e., those that are inputs to user protection-level calculations) assuming that the worst-case

ionospheric condition exists all the time. This approach ensures user integrity; however, it causes a significant loss of availability [1].

In the near future, single-frequency GBAS will evolve to support CAT II/III precision approach under the "GAST-D" requirements framework [2]. In this architecture, the airborne system shares the responsibility for mitigating the ionospheric threat in order to avoid the conservatism of CAT I GBAS and to make it possible to meet more stringent requirements. As part of this process, standardized ionospheric monitors for the airborne system have been proposed and validated. Despite these additions, it is necessary to add additional monitoring within the ground system to retain reasonable availability.

The good news for GBAS, and GNSS in general, is the recent introduction of the L5 civil signal. By receiving measurements on L5 in addition to L1, ionospheric-induced errors will be removed or at least greatly reduced. For a future dual-frequency GBAS, at least two different concepts for measurement smoothing have been proposed: divergence-free smoothing (DFree) and ionosphere-free smoothing (IFree) [3]. Both of these methods have advantages and weaknesses. Divergence-free smoothing does not remove all of the differential ionospheric error. Ionosphere-free smoothing does remove this error entirely (to a first-order approximation), but it introduces additional code-phase error that increases the total receiver noise and multipath error by a factor of 2.6 or more [3,4].

In this paper, we evaluate the performance of dual-frequency GBAS using data collected on L1 and L2. These results highlight the expected performance level when the L5 signal becomes available. The data for this analysis comes mostly from the U.S. CORS (Continuously Operating Reference Stations) network [5]. CORS networks provide dual frequency data (L1 C/A and L2 semi-codeless). After examining data from many receivers within the CORS network, we have selected three small regions, or "clusters," for detailed study. Two of these are in the Conterminous United States (CONUS), while one is in Western Africa and is in the equatorial geomagnetic region. Within these clusters, we chose pairs of receivers separated by several tens of kilometers. One of these receivers is assumed to represent a GBAS ground system, and the other represents a static GBAS aircraft user.

Data evaluation for these "virtual" GBAS installations is based upon observed accuracy, predicted integrity, and potential availability for a GBAS application. The "virtual" ground systems provide differential corrections using DFree and IFree smoothing in addition to conventional single-frequency carrier smoothing (SFCS). "Virtual" airborne systems conduct position estimation by applying these differential corrections and by applying models of the resulting error bounds in their protection level calculations. Accuracy is evaluated by comparing the "virtual airborne" position solution with the known true position of each receiver site. Integrity is evaluated by comparing the resulting position error with the protection level calculated by the "virtual" airborne system. Note that, because virtual user protection levels are based upon error models, this evaluation will primarily illuminate the suitability of these models with respect to the collected data. Finally, availability is estimated from the relationship among position errors, acceptable (bounding) protection levels, and alert limits.

2.0 REVIEW OF DUAL-FREQUENCY SMOOTHING

In this section, we review two types of carrier smoothing algorithms that make use of dual frequency measurements which are proposed in [3].

2.1 GPS Measurement Model

GPS code and carrier-phase measurements on L1 and L2 are modeled as follows.

$$\begin{aligned}
\rho_1 &= R + I_1 + \varepsilon_{\rho 1} \\
\phi_1 &= R - I_1 + N_1 + \varepsilon_{\phi 1} \\
\rho_2 &= R + \frac{f_1^2}{f_2^2} I_1 + IFB + \tau_{gd} + \varepsilon_{\rho 2} \\
\phi_2 &= R - \frac{f_1^2}{f_2^2} I_1 + IFB + \tau_{gd} + N_2 + \varepsilon_{\phi 2}
\end{aligned} \tag{1}$$

where

$\rho_{1(2)}$ = L1 (L2) code phase measurement

$\phi_{1(2)}$ = L1 (L2) carrier phase measurement

R = true geometric range from receiver to satellite, plus errors common among four measurements including receiver and satellite clock error, tropospheric delay.

I_1 = ionospheric delay on L1 frequency

IFB = receiver interfre - frequency bias

τ_{gd} = satellite inter - frequency bias

$N_{1(2)}$ = integer ambiguity term

$\varepsilon_{\rho 1(2)}$ = multipath and receiver noise term on L1 (L2) code phase measurement

$\varepsilon_{\phi 1(2)}$ = multipath and receiver noise term on L1 (L2) carrier phase measurement

It is important to note the contrasting characteristics of code and carrier measurements. Code measurements are free from ambiguities but have multipath and receiver noise errors (ε_ρ) that are usually more than 2 orders of magnitude larger than that of the carrier measurement (ε_ϕ). On the other hand, the less-noisy carrier measurement has an unknown integer ambiguity.

2.2 General Description of Carrier Smoothing

The objective of carrier smoothing is to suppress multipath and receiver noise error on code measurements. This is accomplished by using the low-pass filter illustrated in Figure 1. First, code and carrier inputs are differenced to remove ranging information (receiver to satellite distance) from the filter input, leaving only nuisance terms (errors) that we wish to "smooth out." The resulting measurement is called the *Code-Minus-Carrier* (CMC) measurement, or just "CMC". CMC is fed into the low-pass filter to attenuate multipath and receiver noise error on code measurement. The output from the low-pass filter, $\hat{\rho}$, is recombined with the carrier input to reconstruct the ranging information. Depending on the form of the code and carrier inputs, different types of smoothing are possible [1,2]. In the following sections, we will review the three different types of smoothing examined in this research.

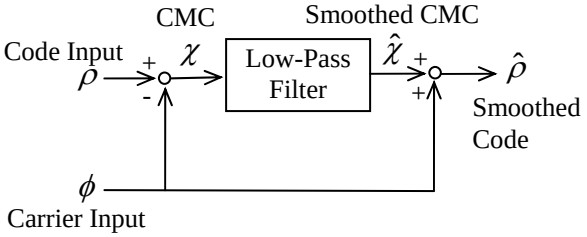

Figure 1: Block Diagram of Carrier Smoothing Filter.

2.3 Single Frequency Smoothing (SFCS)

In conventional single frequency carrier smoothing (SFCS), raw code and carrier measurement are used as inputs. As shown in equation (1), since raw code and carrier measurements have different signs for the ionospheric delay term, CMC (denoted as χ) includes twice the ionospheric delay ($2I_1$):

$$\chi_{SFCS} = \rho_1 - \phi_1 = \varepsilon_{\rho 1} + 2I_1 - N_1 \tag{2}$$

Here, the receiver error term on the carrier measurement (ε_ϕ) is neglected because it is much smaller than the receiver error term on the code measurement (ε_ρ).

By putting CMC into the low-pass filter and recombining the filter output with the carrier input, we obtain smoothed CMC and smoothed code as follows.

$$\hat{\chi}_{SFCS} = \hat{\varepsilon}_{\rho 1} + 2\hat{I}_1 - N_{L1} \tag{3}$$

$$\hat{\rho}_{SFCS} = \hat{\chi}_{SFCS} + \phi_1 = R + \hat{\varepsilon}_{\rho 1} + \left(2\hat{I}_1 - I_1\right) \tag{4}$$

When the amount of ionospheric delay changes with time, the ionospheric delay term in equation (2) yields so-called "code-carrier divergence" and smoothed ionospheric delay. In equation (3), ($\hat{I}_1$) is not identical to the original ionospheric delay (I_1). Therefore, using SFCS, the difference in the rate of change of ionospheric delay between ground and airborne systems yield another source of error in addition to the difference in the amount of ionospheric delay itself.

2.4 Divergence-Free Smoothing (DFree)

Divergence-free smoothing (DFree) resolves part of the problem that exists in SFCS. More specifically, DFree removes the code-carrier divergence effect. Since code-carrier divergence is caused by the fact that the code and carrier inputs have different sign in ionospheric delay, DFree smoothing uses a linear combination of dual-frequency carrier measurements that creates the same sign and amount of ionospheric delay as the raw code measurement. This is accomplished by using following linear combination:

$$\phi = \phi_{L1} - \frac{2}{\xi}\left(\phi_{L1} - \phi_{L2}\right) = R + I_1 + N_{LC,DF} + \frac{2}{\xi}\left(IFB + \tau_{gd}\right) \tag{5}$$

where,

$$\xi = \left(1 - \frac{f_1^2}{f_2^2}\right)$$

$$N_{LC,DF} = N_1 - \frac{2}{\xi}\left(N_1 - N_2\right)$$

By using equation (5) as the carrier input, ionospheric delay is canceled out from CMC, which becomes:

$$\chi_{DFree} = \varepsilon_{L1} - N_{LC,DF} - \frac{2}{\xi}\left(IFB + \tau_{gd}\right) \tag{6}$$

As the CMC input to the low-pass filter does not include ionospheric delay, DFree smoothing is free from the ionospheric divergence which affected SFCS. However, in recombining the smoothed CMC with the carrier input to reconstruct the ranging information, the resulting

smoothed code still includes ionospheric delay, as shown in the following equation.

$$\hat{\rho}_{DFree} = \hat{\chi}_{DFree} + \phi = R + \hat{\varepsilon}_{L1} + I_{L1} \quad (7)$$

Therefore, in DFree smoothing, the difference in the ionospheric delay rate of change rate between the ground and airborne systems is irrelevant, but the difference in the amount of ionospheric delay between ground and air remains and is a potential concern during anomalous ionospheric behavior.

2.5 Ionosphere-Free Smoothing

Ionosphere-Free smoothing (IFree) removes ionospheric delay entirely (to a first-order approximation). To accomplish this, ionosphere-free combinations are used both for code and carrier inputs to the smoothing filter.

$$\rho = \rho_{L1} - \frac{1}{\xi}(\rho_{L1} - \rho_{L2}) = R + \varepsilon_{L1} - \frac{1}{\xi}(\varepsilon_{L1} - \varepsilon_{L2}) + \frac{1}{\xi}(IFB + \tau_{gd}) \quad (8)$$

$$\phi = \phi_{L1} - \frac{1}{\xi}(\phi_{L1} - \phi_{L2}) = R + N_{LC,IF} + \frac{1}{\xi}(IFB + \tau_{gd}) \quad (9)$$

where,

$$N_{LC,IF} = N_1 - \frac{1}{\xi}(N_1 - N_2)$$

As shown in equation (8), using a linear combination of dual-frequency code measurements provides an ionosphere-free code input. However, combining code measurements in this manner increases the receiver error term at the same time.

By subtracting equation (9) from equation (8), we obtain the CMC measurement as follows:

$$\chi_{IFree} = \varepsilon_{L1} - \frac{1}{\xi}(\varepsilon_{L1} - \varepsilon_{L2}) - N_{LC,IF} \quad (10)$$

After smoothing CMC and recombining it with the carrier input, the resulting smoothed code is:

$$\hat{\rho}_{IFree} = \hat{\chi}_{IFree} + \phi = R + \hat{\varepsilon}_{L1} - \frac{1}{\xi}(\hat{\varepsilon}_{L1} - \hat{\varepsilon}_{L2}) + \frac{1}{\xi}(IFB + \tau_{gd}) \quad (11)$$

As shown in equation (11), IFree smoothed code free from ionospheric effects to first-order; but a significant price is paid in terms of higher receiver noise errors. The desirability of IFree thus depends on the degree of ionospheric unpredictability and the magnitude of receiver errors, which themselves are not perfectly known.

3.0 NGS/CORS DATA ANALYSIS APPROACH

3.1 Data Used for Analysis

To investigate dual-frequency GBAS performance, GPS data from the Continuously Operating Reference Stations (CORS) network is used. The CORS network is managed by the U.S. National Geodetic Survey (NGS) and contains more than 1,450 stations throughout the United States, its territories, and a few countries outside the U.S. [4]. GPS data is provided in the Receiver Independent Exchange Format (RINEX) and is freely available directly from CORS website. From the CORS network, we selected three clusters for detailed study after a widespread search for anomalous ionospheric conditions, which were not found during the first half of 2010. Two of the clusters selected are in CONUS, and one is in the West African Country of Benin. The geomagnetic latitude of CONUS is relatively high, therefore ionospheric activity over the CONUS corresponds to "mid-latitude" conditions. On the other hand, Benin is located in the equatorial geomagnetic region and is expected to see more active ionospheric behavior. In each cluster, results for individual two-station pairs are shown. The distances between stations are 10 – 30 km for the CONUS clusters and about 100 km for the Benin cluster. Although the separations in the Benin cluster are longer than desirable, Benin provides the best example of equatorial geomagnetic conditions given the limited number of CORS receivers in this region of the world.

For each CORS station pair, one station is assumed to represent a GBAS ground system, and the other is assumed to represent a static GBAS airborne system. The specific stations used for data analysis are listed in Table 1 along with their approximate position, receiver type, and antenna type.

Table 1: Sites Used for Analysis

Cluster Name	Site ID	Approx. Dist. (km)	Approx. Position (ITRF)			Receiver	Antenna
			Lat. (dd mm ss)	Lon. (dd mm ss)	H (m)		
Memphis	ZME1	10.8	N35° 04’ 02”	W89° 57’ 19”	68.15	NOVATEL WAASGII	MPL WAAS 2225NW
	EDM1		N35° 03’ 31”	W89° 50’ 14”	79.47	LEICA GRX1200GGPRO	LEIAX1202GG
Ohio	OHLO	32.6	N41° 17’ 37”	W82° 13’ 58”	221.30	TRIMBLE NETR5	TRM57971.00
	OHHU		N41° 10’ 36”	W82° 33’ 41”	253.32	TRIMBLE NETR5	TRM57971.00
Benin	BJAB	101.2	N07° 10’ 56”	E02° 00’ 01”	243.75	TRIMBLE NETR5	TRM57971.00
	BJCO		N06° 23’ 04”	E02° 27’ 00”	30.70	TRIMBLE NETR5	TRM59800.00

3.2 GBAS Performance Evaluation Tools

We developed a MATLAB-based tool set to evaluate dual-frequency GBAS performance. This tool set consists of three independent tools:

(1) Receiver Error Modeling Tool

(2) Ground System Emulation Tool

(3) Airborne System Emulation Tool

Figure 2 shows the block diagram of this tool set. Each tool is interfaced using the files shown in this figure, meaning that a file output from one tool serves as an input to another tool. This code structure is a compromise between simulation efficiency, and maintainability, and future expandability.

Receiver Error Modeling Tool

The Receiver Error Modeling Tool generates receiver error models as a function of elevation angle. The resulting models are then used for protection level calculations. This tool is divided into three parts. The first part calculates smoothed code-minus-carrier (SCMC), which is used to estimate receiver noise and multipath errors. Since SCMC has an arbitrary bias due to the carrier integer ambiguity and inter-frequency biases, leveling of the initial SCMC is used to remove this bias so that SCMC comes to have zero mean. The second part of this tool is normalization. The purpose of normalization is to reduce the elevation dependency of SCMC. In the normalization process, standard deviations in each of a set of elevation bins (selected to produce approximately the same number of observations in each bin) are calculated first, and then these standard deviations are fitted to a polynomial function of elevation angle. Normalization of each error estimate is then carried out based on this polynomial function. The third part, overbounding, determines an inflation factor such that the actual normalized SCMC is bounded by a zero-mean Gaussian distribution with a standard deviation increased by this factor. Finally, the receiver error model is determined from a curve which is obtained by interpolating the resulting inflated standard deviations.

Ground System Emulation Tool

The Ground System Emulation Tool calculates pseudorange corrections using known antenna positions and satellite navigation data. Pseudorange corrections are calculated for the three types of smoothing defined in Section 2.0: SFCS, DFree, and IFree.

Airborne System Emulation Tool

The Airborne System Emulation Tool calculates user position solutions and protection levels. When calculating position solution, the differential corrections provided by the Ground System Emulation Tool are applied. In protection level calculations, receiver error models provided by the Receiver Error Modeling Tool are used to bound ground and airborne receiver errors.

4.0 RANGE DOMAIN ANALYSIS

4.1 Receiver Error (Multipath and Receiver Noise)

The magnitude of receiver errors largely depends on the local environment as well as the receiver and antenna type. During our simulation, we encountered significant differences in receiver error among CORS sites. Figure 3 shows the standard deviation of receiver error in each elevation bin. We used a 5 degree elevation bin width up to 70 degrees, followed by a 7.5-degree bin width (70.0 - 77.5 deg) and a 12.5-degree bin width (77.5 – 90.0 deg). Wider widths in higher elevation bins were used to reduce the difference in the number of samples in each bin.

Figure 4 shows the ratio of receiver error magnitude between IFree and DFree smoothing. We discovered that IFree smoothing yields 3 to 4 times larger errors than DFree smoothing. This result is larger than the theoretical ratio of 2.978 obtained by assuming that L1 and L2 errors are statistically independent and identically distributed.

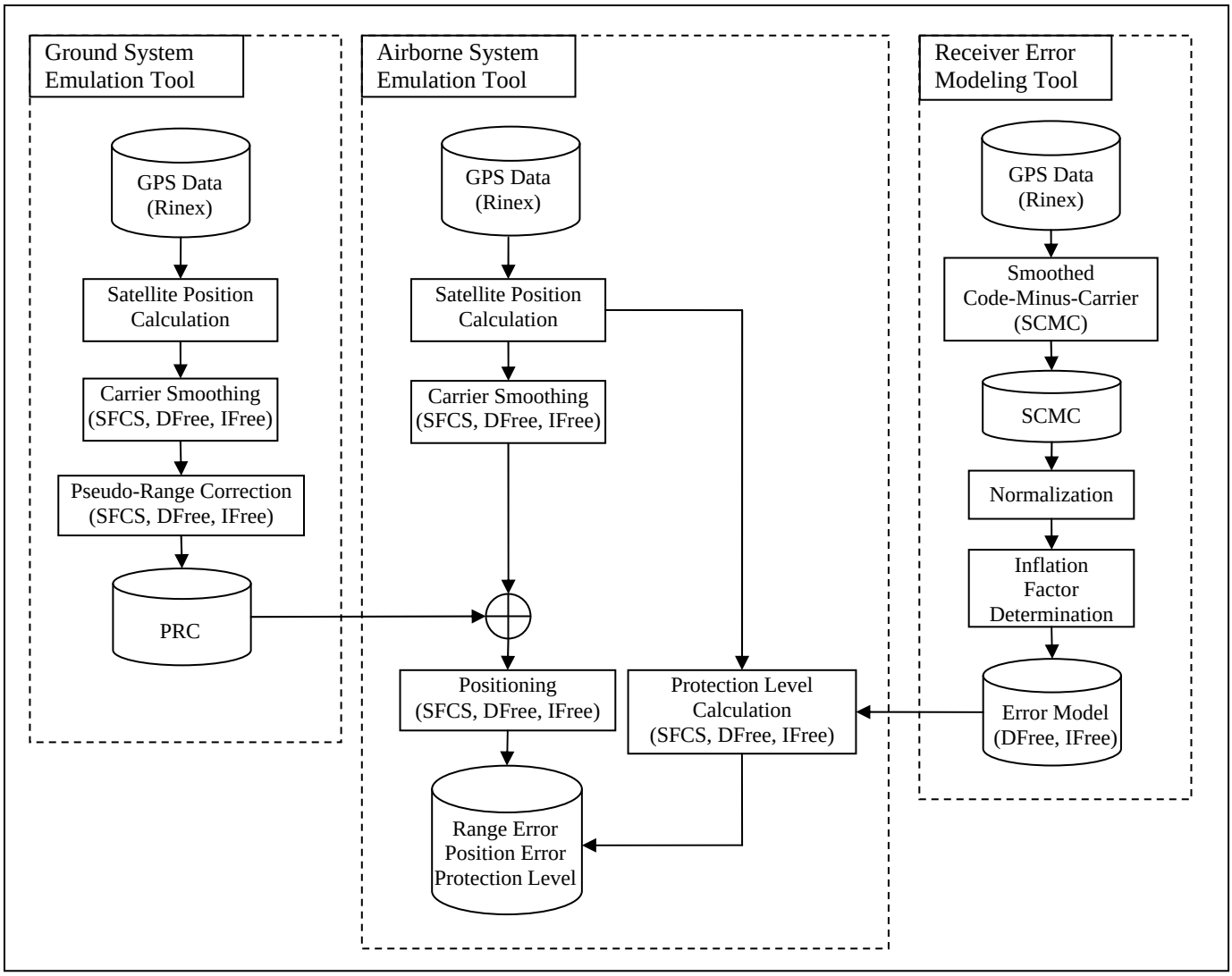

Figure 2: Block Diagram of Dual-Frequency GBAS Performance Evaluation Tool.

This result held for all receiver sites examined, despite the fact that different sites had very different receiver errors. Note that this result is obtained based on the L1 code and L2 semi-codeless measurements available in CORS data. Dual-frequency GBAS will likely combine L1 with the new L5 civil signal, which resides within a protected aeronautical radionavigation service (ARNS) band, has a 10-times-higher chipping rate and a 3-dB-higher transmission power compared to the L1 signal. Thus, IFree with the L1/L5 combination is expected to have smaller receiver error compared to the results obtained in this paper.

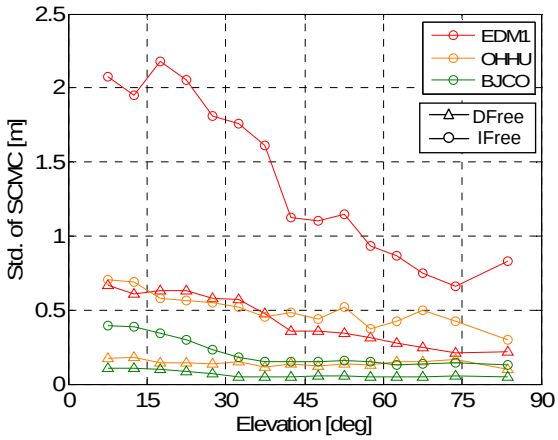

Figure 3: Standard deviation of receiver error in each elevation bin for different sites and smoothing algorithms.

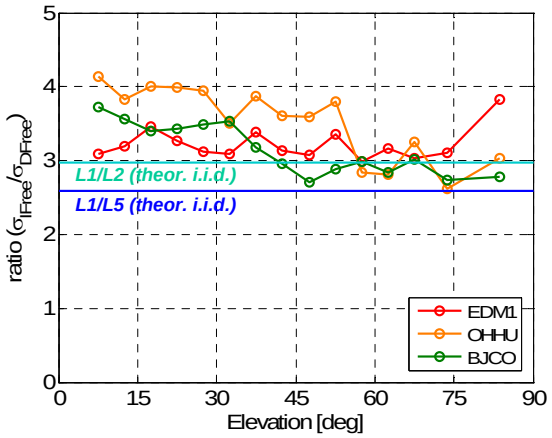

Figure 4: Receiver error ratio between DFree and IFree smoothing

5.0 POSITION DOMAIN ANALYSIS

5.1 VPL Equation

In the GBAS integrity concept, integrity risk is divided into three categories, i.e. risk under fault-free conditions (H0), risk under the single-reference-receiver failure condition (H1), and all other risks not covered by the H0 and H1 risks (H2). Since faults are rarely encountered in data analysis, we focused on the fault-free condition (H0) in this research.

In conventional single-frequency GBAS, the VPL equation for the nominal (H0) condition is standardized as follows [7]:

$$VPL_{H0} = K_{ffmd}\sqrt{\sum_{i=1}^{N} s_{vert,i}^2 \sigma_i^2} \qquad (12)$$

$$\sigma_i^2 = \sigma_{gnd,i}^2 + \sigma_{air,i}^2 + \sigma_{iono,i}^2 + \sigma_{tropo,i}^2 \qquad (13)$$

In equation (12), K_{ffmd} is the multiplier derived from the probability of fault-free missed detection; $s_{vert,i}$ is the vertical component of the projection matrix for the i^{th} satellite, which is used in the position calculation; and N is the number of satellites in the position solution.

Equation (13) includes four terms, each of which express 1-σ error bounds on from different error sources in the range domain. σ_{gnd} and σ_{air} are the standard deviations that bound the ground receiver and airborne receiver error respectively. For conventional single-frequency GBAS, there are standard error models to describe these ground and airborne receiver error terms [7]. However since there is no standard model for dual-frequency GBAS, we constructed receiver error models using the actual CORS data. This approach provides more realistic performance estimates for the particular CORS sites being studied. The resulting error models are shown in the next section.

σ_{iono} bounds residual error caused by ionospheric delay under non-anomalous ionospheric conditions [6]. We used three deferent equations for this term depending on smoothing type, as shown below:

$$\begin{cases} \sigma_{iono,SFCS} = F_{pp} \times \sigma_{vig} \times \left(x_{air} + 2 \times \tau \times v_{air}\right) \\ \sigma_{iono,DFree} = F_{pp} \times \sigma_{vig} \times x_{air} \\ \sigma_{iono,IFree} = 0 \end{cases} \qquad (14)$$

Here, F_{pp} is the obliquity factor to convert vertical or zenith errors into slant errors at a particular elevation angle [7], σ_{vig} is the standard deviation of a normal distribution associated with the residual ionospheric uncertainty due to non-anomalous spatial decorrelation, x_{air} is the separation between ground and airborne receivers, τ is the carrier smoothing time constant, and v_{air} is the horizontal speed of the aircraft. We used 4 mm/km, which is the one suggested as an appropriate value for CONUS, as the value for σ_{vig} [6]. We assumed 70 m/sec of airborne speed, corresponding to a typical jet-aircraft approach velocity, and we used the same smoothing time constant of 100 sec as the existing single-frequency GBAS.

For SFCS, we used the same VPL equations as for single-frequency GBAS, which include both the spatial separation term (x_{air}) and the code-carrier divergence term ($2\ \tau\ v_{air}$) in equation (14). For DFree, we eliminated the code-carrier-divergence term. For IFree, we eliminated both terms (i.e., $\sigma_{iono} = 0$) since we are using ionosphere-free measurements.

5.2 Results

Modeled Receiver Error

As explained in Section 3.2, receiver error models were constructed for each CORS receiver based on the actual data. The one-sigma value in each elevation bin was inflated so that a zero-mean Gaussian distribution with the inflated sigma overbounds the actual error distribution in the tail visible in the data. Figure 5 illustrates how the amount of inflation was determined. The dotted lines in the figure are probability densities (PDFs) of normalized error from the data. As discussed in Section 3.2, we normalized the actual estimated error in order to reduce elevation-angle dependency. In Figure 5, the PDFs of example zero-mean Gaussian distributions with standard deviations of 1.5 – 2.1 are plotted along with the actual distributions. By looking at this type of plot, we empirically determined the amount of inflation necessary

to bound the actual data. In this example, we decided to employ an inflation factor of 2.0 for both DFree and IFree.

Figure 6 through Figure 8 show estimated receiver errors for three CORS sites, indicating the significant difference in errors among these sites. EDM1 receiver error (Figure 6) is considerably worse than the other two sites. While some error variation is expected among CORS sites, this degree of difference is well beyond our expectations. For EDM1, the modeled errors are worse than the standard GAD-A curve both for DFree and IFree. In fact, the model for IFree is far worse than GAD-A. Although receiver errors this high are not practical for GBAS, this site was mostly used for purposes of comparison.

The receiver error at OHLO (Figure 7) is much lower than EDM1. Although the error model for IFree is still worse than the GAD-A curve, the model for DFree is quite close to the GAD-C curve. Furthermore, the receiver error at BJCO (Figure 8) is much lower than at OHLO. The resulting error model for DFree was better than the GAD-C curve with margin, while the IFree error model was compatible with GAD-B curve. This result suggests that, with further antenna and siting optimization, even IFree-based GBAS is likely to be feasible.

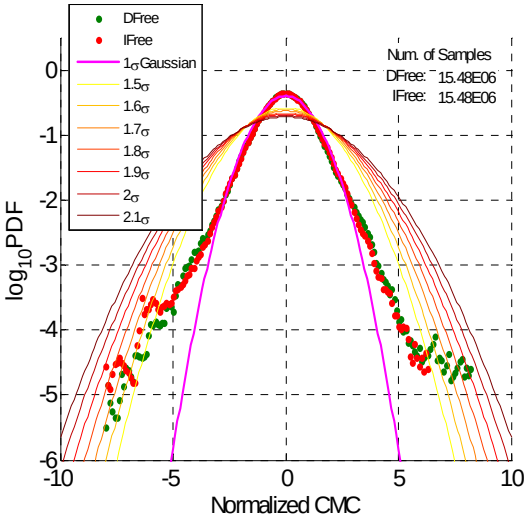

Figure 5: An example of overbounding via sigma inflation

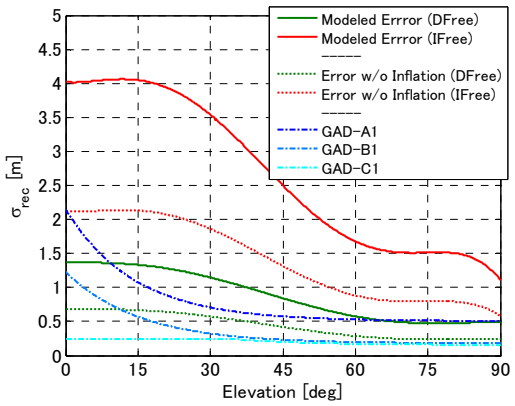

Figure 6: Receiver Error Model for EDM1 (High Error Environment)

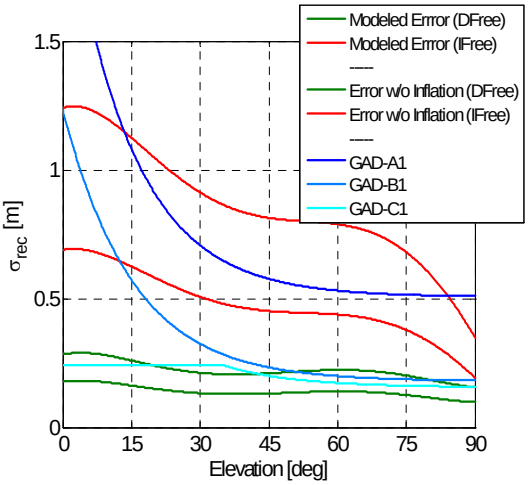

Figure 7: Receiver Error Model for OHLO (Moderate Error Environment)

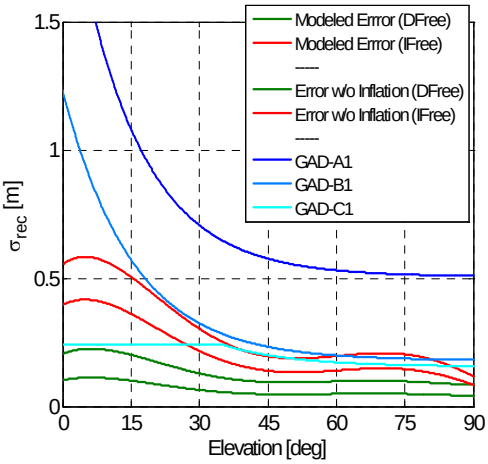

Figure 8: Receiver Error Model for BJCO (Low Error Environment)

Accuracy

Figure 9 through Figure 11 show 95 % vertical accuracy for the three clusters. These results are based on position solutions using all-in-view satellites from the current GPS constellation, meaning the constellation that was present at the time the data was taken (in early to mid-2010). Reflecting the different receiver error characteristics observed in the previous section, each cluster achieved varying levels of accuracy.

In the high error environment (Memphis Cluster, Figure 9), the accuracy based on DFree is slightly better than the CAT-III accuracy requirement, while that based on IFree falls far short of the CAT-I requirement. In the moderate error environment (Ohio Cluster, Figure 10), DFree accuracy is better than the CAT-III requirement with margin, and IFree accuracy is in the vicinity of the CAT-III requirement. Note that the days surrounded by the dashed rectangle showed less accuracy compared to other days. This appears to have resulted from the fact that Block IIR-M Satellites were not usable (L2 measurements were not available in the CORS data sets), which made the usable satellite constellation weak.

As expected, better accuracy was obtained in the low error environment (Benin Cluster, Figure 11). In this environment, even IFree-based accuracy achieved the CAT-III requirement with more than 1 meter of margin. This result revealed that, with the current "full" GPS constellation, meeting the GBAS CAT-III vertical accuracy requirement is not difficult.

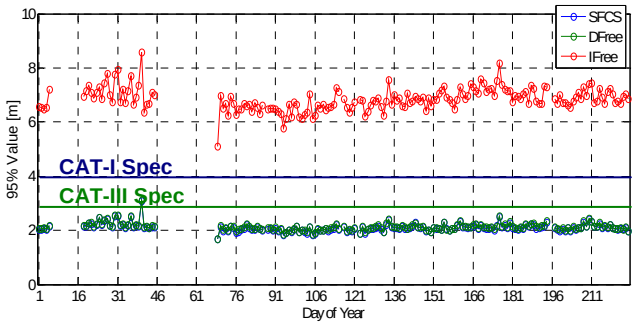

Figure 9: 95 % Vertical Accuracy for Memphis cluster from 1 January –13 August 2010 (High Error Environment)

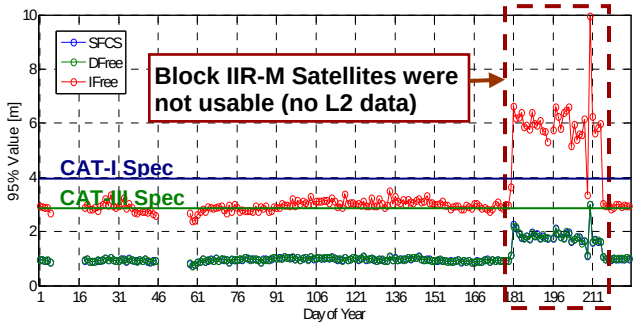

Figure 10: 95 % Vertical Accuracy for Ohio Cluster from 1 January –13 August 2010 (Moderate Error Environment)

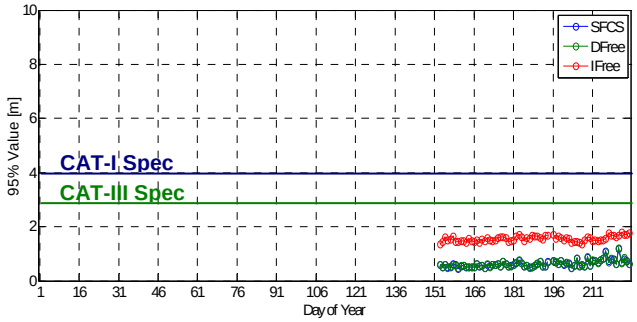

Figure 11: 95 % Accuracy for Benin Cluster during the period of 1/1 – 8/13, 2010 (Low Error Environment)

Integrity

Table 2 includes triangle plots of observed errors vs. computed VPLs for all three clusters and three types of smoothing. In calculating SFCS and DFree VPLs for these charts, we assumed the same baseline distance for Memphis and Benin cluster as Ohio cluster so that we can directly compare VPLs among clusters. Without assuming the same distance, longer baselines result in larger VPLs due to the σ_{iono} term in the VPL equation. Note that this artificial shortening of the actual baselines changes (and reduces) VPL but does not change the actual position errors resulting from the data.

In these charts, points in the upper-left-section, where VPL is larger than the actual vertical error, are expected and mean that integrity was maintained. For all cases, no integrity failures were observed during our examination. From these results, although the number of samples is limited to more than 2×10^5 for the two CONUS clusters and more than 2×10^5 for the Benin cluster, it appears that our approach to error modeling and determining σ_{pr_gnd} is appropriate.

On the whole, the charts for SFCS and for DFree look quite similar, with some VPL improvement in the DFree

Table 2: Triangle Plots for three clusters using three types of smoothing.

Cluster	SFCS	DFree	IFree
Mem-phis	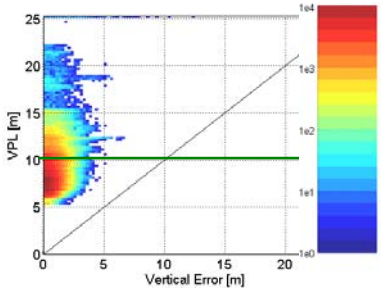	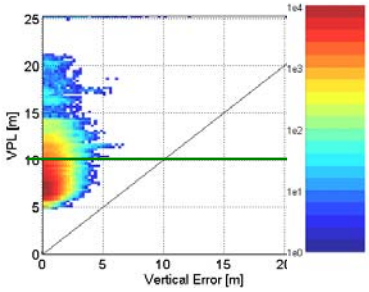	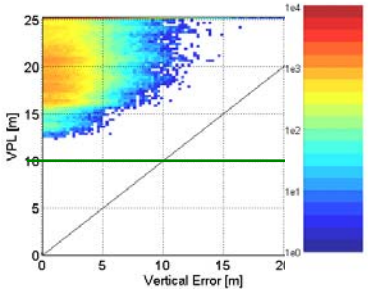
Ohio	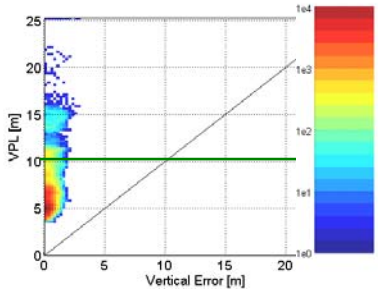	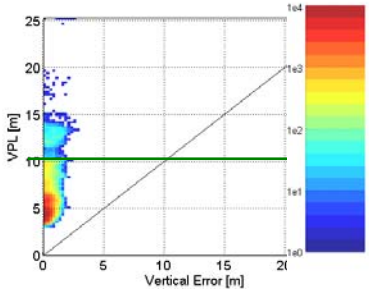	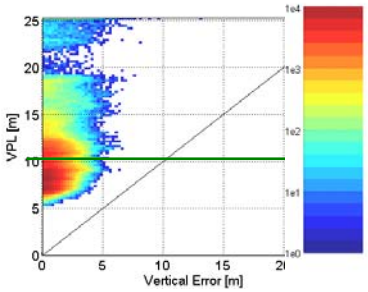
Benin	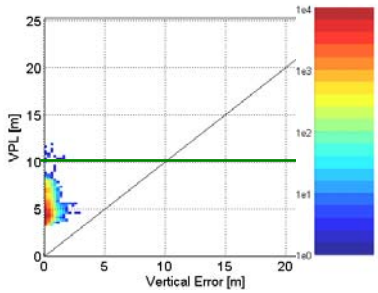	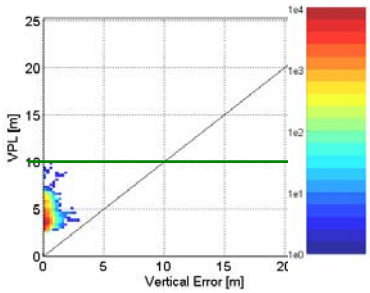	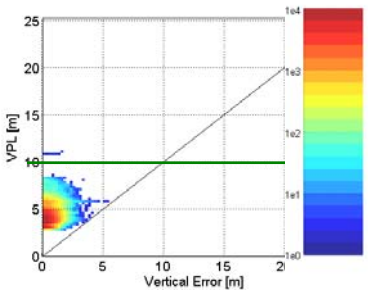

cases. This improvement in VPL is due to elimination of the divergence term in the σ_{iono} equation, as shown in equation (14). The charts for IFree are significantly different from the other two cases. In particular, both VPL and vertical error vary widely for IFree in comparison to the SFCS and DFree cases. This is due to the larger receiver errors inherent in IFree smoothing.

In the SFCS and DFree charts, the VPL margin over actual errors is relatively large due to the inclusion of the σ_{iono} term in VPL equation. In the IFree charts, this term is zero, and the margin becomes much smaller, although integrity is maintained.

Availability

Table 3 summarizes the availability for each cluster using the different smoothing methods. We assumed a Vertical Alert Limit (VAL) of 10 meters and considered epochs in which VPL is less than VAL as available. For all three clusters, DFree achieved the highest availability, as expected. One interesting results is that even IFree achieved more than 99.9 % availability in the Benin cluster, where the modeled receiver error was compatible with the GAD-B error model. From this result, given the current constellation of more than 30 GPS satellites, IFree-based GBAS seems feasible.

Table 3: Availability for each cluster assuming VAL = 10 meters

Receiver Error (Multipath + Noise)	Cluster Name	Availability (VPL<VAL) VAL=10 (m)		
		SFCS	DFree	IFree
High	Memphis	0.71343	0.796625	0.00000
Moderate	Ohio	0.94711	0.97516	0.60552
Low	Benin	0.99946	0.99993	0.99949

SUMMARY AND FUTURE WORK

The original goal of this work was to examine how dual-frequency smoothing behaved under unusual ionospheric conditions observed in actual data. Since no such unusual conditions were observed in the first half of 2010, the focus turned toward examining performance under nominal conditions at different CORS sites. While the degree of nominal-error variation among CORS sites was greater than expected, a subset of these sites in Benin and Ohio demonstrated receiver noise and multipath errors at least potentially compatible with the requirements of CAT III GBAS. Since GBAS utilizes antennas designed to tighter specifications and implements tighter antenna siting constraints, it is expected that future dual-frequency GBAS equipment will be able to support 99.9% availability for CAT III operations with IFree smoothing. Availabilities of 99.99% or higher will likely require DFree smoothing or the "hybrid" approach described in [4].

While no ionospheric anomalies were found in a search of CORS data during 2010, it is expected that anomalies will occur during and shortly after the peak of the upcoming solar cycle. Thus, repeating this analysis once anomalies are found in recorded data will help demonstrate the robustness of dual-frequency smoothing. In addition, the future use of coded signals on L5 or L2C instead of the semi-codeless measurements used here will be much more representative of future dual-frequency GBAS, and it should give better results. Finally, as more data under varied ionospheric conditions is collected, it can be tested with a wider range of potential smoothing algorithms (see [8]) to determine if alternatives to IFree and DFree offer significant additional benefits to dual-frequency GBAS.

ACKNOWLEDGMENTS

The authors would like to thank the many people at Stanford, NEC, and the FAA who helped with this work. They would also like to acknowledge the funding support of NEC Corporation and the FAA Satellite Navigation Program Office. However, the opinions expressed here are solely those of the authors.

REFERENCES

[1] S. Pullen, Y.S. Park, and P. Enge, "Impact and Mitigation of Ionospheric Anomalies on Ground Based Augmentation of GNSS," *Radio Science*, Vol. 44, Aug. 8, 2009. http://www.agu.org/journals/rs/rs0904/2008RS004084/2008RS004084.pdf

[2] T. Murphy and S. Naerlich, "Development Baseline SARPs Proposal," ICAO Navigation Systems Panel (NSP) WGW Meeting, NSP May 10 / Flimsy 29, Montreal, Canada, May 17-28, 2010. http://www.icao.int

[3] P. Hwang, G. McGraw, and D. Bader, "Enhanced Differential GPS Carrier-Smoothed Code Processing Using Dual- Frequency Measurements," *NAVIGATION*, Vol. 46, No. 2, Summer 1999, pp. 127-138. http://www.ion.org/search/view_abstract.cfm?jp=j&idno=2250

[4] H. Konno, "Design of an Aircraft Landing System using Dual-Frequency GNSS," Ph.D. Dissertation, Dept. of Aeronautics and Astronautics, Stanford University, Dec. 2007. http://waas.stanford.edu/~wwu/papers/gps/PDF/Thesis/HiroKonnoThesis07.pdf

[5] Continuously Operating Reference Station (CORS) Website, U.S. National Geodetic Survey. http://www.ngs.noaa.gov/CORS/

[6] J. Lee, S. Pullen, S. Datta-Barua, P. Enge, "Assessment of Ionosphere Spatial Decorrelation for Global Positioning System-Based Aircraft Landing Systems", *AIAA J. of Aircraft*, Vol. 44, No. 5, Sept.-Oct. 2007, pp. 1662-1669. http://www.aiaa.org

[7] *Minimum Operational Performance Standards for GPS Local Area Augmentation System Airborne Equipment*. Washington, D.C., RTCA SC-159, WG-4, DO-253C, Dec. 16, 2008. http://www.rtca.org

[8] G. McGraw, "Generalized Divergence-Free Carrier Smoothing with Applications to Dual Frequency Differential GPS," *Navigation*, Vol. 56, No. 2, Summer 2009, pp. 115-122. http://www.ion.org/search/view_abstract.cfm?jp=j&idno=2492